Estimating Kinetic Parameters for the Spontaneous Polymerization of Glycidol at Elevated Temperatures

Maximilian E. R. Weiss,* Florian Paulus, Dirk Steinhilber, Anatoly N. Nikitin, Rainer Haag, Christof Schütte*

The ring-opening polymerization of glycidol at elevated temperatures is investigated. To improve the synthesis of dendritic polyether polyols, experiments are carried out without initiator to identify the influence of thermal side reactions. This results in a step-growth polymerization caused by the spontaneous combination of monomers. Kinetic parameters of the side reactions are estimated by fitting simulated number- and weight-average molecular weights to the experimental values measured at different reaction times during the polymerization. The reactions are conducted at three different temperatures of 90, 105, and 120 °C. It is shown that thermal side reactions lead to high dispersities of the final product and are highly sensitive to the reactor operating temperature.

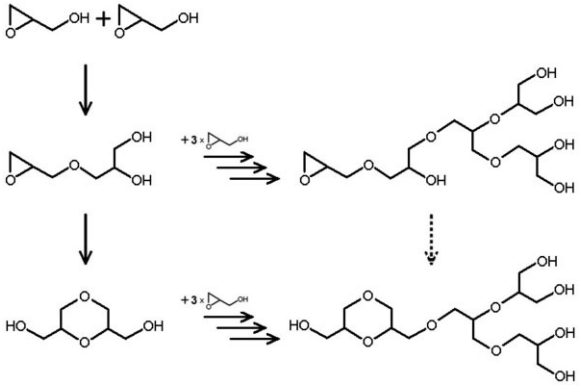

1. Introduction

Polymerization of glycidol (2,3-epoxy-1-propanol) leads to the formation of dendritic polyether polyols (polyglycerol, *d*PG) with a complex and very interesting architecture, consisting of a highly flexible aliphatic polyether backbone and numerous hydroxyl end groups.[1] This material shows excellent biocompatibility and good water solubility. It is used as scaffold in various fields, such as the synthesis of nanocapsules, soluble support for catalysts, biomineralization, protein-resistant surfaces, polymer therapeutics, and diagnostics.[2–5]

In contrast to perfect dendrimers, dendritic polymers (also called hyperbranched polymers) consist not only of branched but also linear subunits.[6,7] This alters the properties of the polymers because the functional groups are not exclusively located on the surface of the molecule; however, with a high degree of branching they are still very useful for most of the applications. On the other hand, dendrimers have to be synthesized in a time consuming, multi-step procedure, whereas the dendritic equivalent can be synthesized in a one-pot reaction within a day.

With the rising interest in dendritic molecules over the last 20 years, the polymerization of glycidol has become an attractive field of research, even though its use as a

M. E. R. Weiss, C. Schütte, A. N. Nikitin
Institut für Mathematik und Informatik, Freie Universität Berlin, Arnimallee 6, 14195 Berlin, Germany
E-mail: maximilian.weiss@fu-berlin.de, christof.schuette@fu-berlin.de
F. Paulus, D. Steinhilber, R. Haag
Institut für Chemie und Biochemie, Freie Universität Berlin, Takustraße 3, 14195 Berlin, Germany
A. N. Nikitin
Institute on Laser and Information Technologies, Svyatoozerskaya 1, Shatura, Moscow Region, 140700, Russia

DOI: 10.1002/mats.201200003

monomer has been known for more than 50 years. In 1966, Sandler and Berg[8] firstly described the polymerization of glycidol in the presence of bases. Almost two decades later, Vandenberg[1] identified reactions resulting in the formation of branched architectures. In the 1990 s, Tokar et al.[9] and Dworak et al.[10] reported the cationic polymerization of glycidol. They elaborated the coexistence of the active chain end (ACE) and activated monomer (AM) mechanisms that lead to the formation of randomly branched polyglycerol. Sunder et al.[11] were the first to develop a controlled synthesis of *d*PG using glycidol as a cyclic, latent AB_2 monomer that is slowly added to trifunctional B_3 core molecules [partially deprotonated 1,1,1-tris(hydroxymethyl)propane]. This was a crucial improvement to the well-known AB_m random polycondensation described by Flory.[12] The potential of the slow monomer addition (SMA) technique coupled with the introduction of multifunctional initiators to control and improve the average molecular weight, dispersity, and the degree of branching of the dendritic polymers was shown analytically by Radke et al.[13] and through a Monte-Carlo simulation by Hanselmann et al.[14] Over the last 10 years, the procedure described above was constantly improved by different work groups.[3] The usual synthesizing process can be divided in the following three steps: (i) multifunctional initiators are partially deprotonated using a base. (ii) Glycidol is slowly added to the running, well-stirred reactor at a fixed temperature. (iii) The final polymer mixture is deactivated using a cationic ion exchange resin. Ideally monomers only bind to the initiators or the growing polymers, in which case the average molecular weight of the final product can be easily controlled by varying the ratio of monomers to initiators.[11] However, if the targeted molar mass is high (exceeding 10 kDa), free monomers accumulate and combine spontaneously at higher temperatures. This increases the number of growing polymer chains in the system and therefore directly leads to a lower average molecular weight.[15] Thus, the thermally induced ring-opening reactions limit the controllability of the synthesis. This paper investigates the influence of monomer combination reactions by performing batch reactions without initiators. With this method the thermally induced ring-opening reactions can be analyzed independently. The underlying process is modeled mathematically and kinetic parameters are calculated by comparison of experimental data to simulations. How simulation studies can improve existing polymerization processes was discussed before by Ray[16] and Busch et al.[17]

For the purpose of modeling and simulating the process the software package PREDICI[18,19] has been used; a state-of-the-art tool optimized for polymerization processes which is well known in the polymer science community. It has been applied successfully to many different polymerization processes.[18] The model developed with the estimated kinetic parameters provides a basis for further simulations of the glycidol polymerization using a variety initiators. With the knowledge gained about the thermal reaction coefficients this more complex process can be improved with mathematical optimization procedures that require a low number of unknown variables. Therefore, we developed a model which could accurately reproduce the experimental results and yet was simple enough for an extended model to be used for high throughput simulations.

2. Experimental Section

2.1. Materials

All chemicals were purchased from Acros Organics and used as received if not described differently. Glycidol was dried over CaH_2 and distilled under reduced pressure. The purified monomer was stored at 4 °C under inert atmosphere. All solvents were purchased from Sigma-Aldrich and used without further purification. All deuterated solvents were obtained from Deutero GmBH and used as received.

2.2. Polymerization

The polymerization was carried out similar to a procedure reported previously.[2,20] In short, 100 g of the dried glycidol was mixed with 225 mL dry tetrahydrofuran (THF) to obtain the monomer solution. A well-dried reactor was used as reaction vessel ($V = 1$ L), equipped with 10 mL dried *N*-methylpyrrolidone (NMP). The monomer mixture was added slowly and constantly over a period of 18 h using a precision dosing pump to the well-stirred reactor (anchor stirrer). In constant intervals of 2 h, the reaction mixture was probed using a pipette and a sample of approximately 0.3 mL was extracted. The samples were collected in 30 mL vials and the solvent was evaporated under reduced pressure. Characterization was performed using gel permeation chromatography (GPC), matrix-assisted laser desorption/ionization time-of-flight mass spectrometry (MALDI-TOF MS), and NMR. The polymerization was carried out at three different temperatures of 90, 105, and 120 °C.

Dendritic polyglycerol: ^{1}H NMR (700 MHz, CD_3OD, δ): 4.00–3.20 (m, *d*PG backbone). ^{13}C NMR (175 MHz, CD_3OD, δ): 82.0–81.0 (*d*PG backbone, linear 1–3 units), 80.5–79.5 (*d*PG backbone, dendritic units), 74.5–73.5 (*d*PG backbone, linear 1–4 units), 73.5–72.0 (*d*PG backbone, terminal/dendritic units), 72.0–70.5 (*d*PG backbone, linear 1–3/1–4 units), 68.4 (s, $C_6H_6-O-\underline{C}H_2-CH_2-O-$), 65.0–64.0 (*d*PG backbone, terminal units), 63.5–62.0 (*d*PG backbone, linear 1–3).

2.3. GPC

Molecular weight distributions were determined by means of GPC coupled to a refractive-index detector obtaining the complete distribution [$\overline{M}_n$, $\overline{M}_p$, $\overline{M}_w$, polydispersity index (PDI)]. Measurements were carried out under highly diluted conditions (10 mg · mL^{-1}, injected volume 20 μL) from an GPC consisting of an Agilent 1100 solvent delivery system with isopump, manual

injector, and an Agilent 1100 differential refractometer. Three 30 cm columns (Polymer Laboratories PLgel Mixed C, 5 μm particle size) were used to separate polymer samples using water as mobile phase at a flow rate of 1.0 mL · min^{-1}. The columns were held at room temperature and with a differential refractometer at 50 °C. WinGPC Unity from PSS was used for data acquirement and interpretation.

2.4. MALDI-TOF MS

Polymer masses were analyzed by MALDI-TOF-MS using an Ultraflex-II TOF/TOF instrument (Bruker Daltonics, Bremen, Germany) equipped with a 200 Hz solid-state smart beam laser. The mass spectrometer was operated in the positive linear mode. MS spectra were acquired over an m/z range of 500–5000. α-Cyano-4-hydroxycinnamic acid (CHCA) was used as the matrix and samples were spotted using the dried droplet technique.

2.5. NMR

NMR spectra were recorded on a Delta Jeol Ecplise 700 MHz spectrometer. Proton and carbon NMR were recorded in ppm and were referenced to the indicated deuturated solvents. NMR data was reported as follows: chemical shift, multiplicity (s = singlet, d = doublet, t = triplet, q = quartet), integration. Multiplets (m) were reported over the range at which they appear at the indicated field strength.

3. Modeling and Simulations

3.1. Basic Model Components

In order to simulate the polymerization process without initiator, the substances we have to consider are glycidol as monomer and NMP as a solvent. The solvent THF used to dilute the monomer was not modeled since it was immediately distilled from the reactor. Therefore, its contribution to the volume in the reactor was negligible. Changes in volume and mass have been taken into account by assigning molecular weights and densities to the elemental species and the polymers.

3.2. Ring-Opening Reactions

The thermally induced ring-opening reaction is based on the fact that any hydroxyl group can react with an epoxide ring as long as the energy input (e.g., by temperature) is high enough. Therefore, we differentiate molecules by the number of epoxide rings and hydroxyl groups they contain. A ring-opening reaction results in the creation of an ether linkage and, depending on which bond in the ring is broken, primary (−CH_2−OH) and secondary hydroxyl group [−(CH−OH)−] arise.[10] This leads to the consumption of one epoxide ring whereas the total number of hydroxyl groups is preserved. In this study we do not differentiate between primary and secondary hydroxyl groups because they are assumed to have the same reactivity. Scheme 1 shows the general mechanism for the ring-opening reaction of glycidol with an alcohol.

3.3. Cyclic Latent AB_2 Random Polymerization

Sunder et al. described glycidol as a cyclic latent AB_2-type monomer,[11] whereby there are two types of functional groups, an epoxide derivative termed A group and a hydroxyl group called B. Since the reactivity of a molecule is dictated by the number of epoxide rings and hydroxyl groups, we will refer to glycidol as AB_1 molecule instead of cyclic latent AB_2-type.

When the A group of a monomer reacts with the B group of another monomer, a dimer with one A and two B groups is formed. This polyaddition is illustrated in Scheme 2.

The product can react with other monomers or polymers which results in a step-wise growth of the polymers. In general, an AB_s molecule can react with an AB_r one to form an AB_{s+r} polymer and the A groups can react with any of the B ones to form a dendritic structure. Such reactions are commonly used to describe AB_m random condensation processes which have already been investigated thoroughly by Flory.[12] Furthermore, Radke et al.[13] and Hanselmann et al.[14] have described ways to improve such a synthesis with respect to the average molecular weight and the dispersity of the final product.

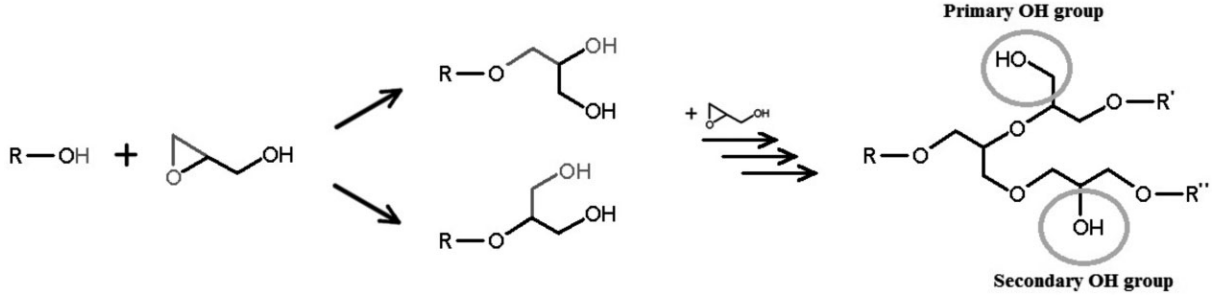

Scheme 1. Reaction of an alcohol with a glycidol monomer. The epoxide ring reacts with the hydroxyl group forming an ether linkage while preserving the overall number of hydroxyl groups. Polymers created this way contain primary and secondary hydroxyl groups.

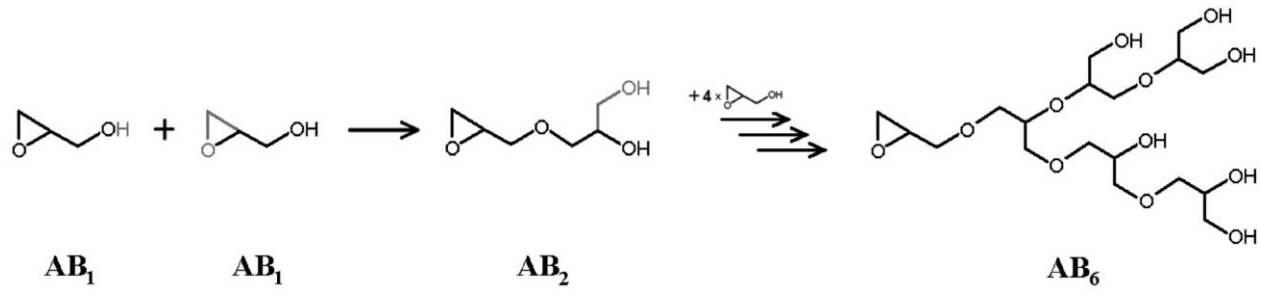

Scheme 2. Ring-opening reaction scheme for two glycidol monomers forming an AB_2 dimer (glycidly glycerine). By binding more monomers a dendritic polymer AB_n (e.g., $n = 6$) is created.

3.4. Cyclization Reactions

So far, only intermolecular ring-opening reactions have been discussed, but AB_m polymers can react in three different ways: (a) its A group combines with a B group of another molecule; (b) its B group combines with the A group of another molecule; (c) its A group reacts with one of the B groups located on the same molecule. The first two reaction pathways (a) and (b) lead to the well-known step-growth polymerization, but the third one (c) results in the formation of a macromolecular cycle. The importance of such reactions has already been shown by Burgath et al.,[15] but these reactions have still not been modeled explicitly. An intramolecular reaction (c) can be expected to occur eventually because of the high reactivity of epoxide derivatives and the fact that the closest hydroxyl groups are the ones located on the same molecule. While the number of B groups remains unchanged by the cycle formation, the A group is consumed and a cyclic polymer can no longer bind to the B group of another molecule with pathway (a). Thus, it can only react according to the above mentioned reaction pathway (b). Polymers that have undergone cycle formation will be referred to as B_s molecules with the subscript denoting its size. Scheme 3 shows a typical cyclization reaction of a dimer.

Before a cycle can be formed, the polymer has to bend and take a certain conformation so that the A and B groups can come in contact. Therefore, the kinetic rate at which cycles are formed may depend on the size of the reacting molecule. Up to this point, there is no sound theory about the chain-length dependency of cyclization rates based on intramolecular ring-opening reactions of dendritic polymers. The common theory about linear, randomly coiling polymers resulting from polycondensation reactions,[21] cannot be applied to branched polymerization as the Gaussian end-to-end distance assumption is not applicable. In addition, the ring size also depends on monomer structure, reaction radius of the monomer, etc.[22] Based on the available literature data, it is not possible to get reliable information about the chain-length dependence law for the cyclization rate coefficient for our system. Therefore, a simplified model was used according to which the reaction of an epoxide with a hydroxyl group did not depend on the chain length that connected them. Since every hydroxyl group can lead to the formation of a cycle, the probability of a cyclization is proportional to the number of hydroxyl groups on the reacting polymer and the coefficient is multiplied by that number. However, a monomer cannot undergo cyclization because its structure is not flexible enough.

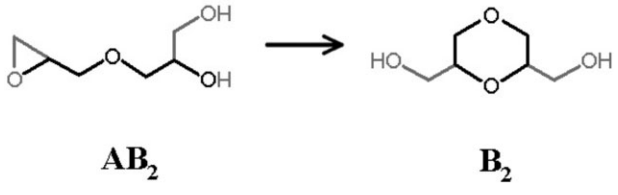

Scheme 3. A typical cyclization reaction. The smallest cycle that can be formed is illustrated here.

3.5. Simulation by PREDICI

For our simulations we used the software package PREDICI to calculate the concentration changes for each species involved by solving a large set of nonlinear, coupled differential equations based on population balance theory.[18,19,23] As described in the previous section, the product of the ring-opening polymerization is AB_s and polymers that have undergone cyclization B_s. The subscript denotes the number of hydroxyl groups of the molecules and is equivalent to the number of monomers that were incorporated in the polymers. Monomers are defined as polymers of size 1 and are written as AB_1.

The system of reaction equations for the thermally induced ring-opening polymerization of glycidol can be written as follows

$$AB_s + AB_r \xrightarrow{k_p \cdot (s+r)} AB_{s+r} \quad (1)$$

$$B_s + AB_r \xrightarrow{k_p \cdot s} B_{s+r} \quad (2)$$

$$AB_s \xrightarrow{k_c \cdot s} B_s \quad (3)$$

$$* \xrightarrow{k_{feed}(t)} AB_1 \quad (4)$$

The subscripts denoting the size of the involved polymers can take any value greater than or equal to 1. Reaction (3) shows the cyclization reaction which poses an exception where the subscript must be greater than 1. The rate of every reaction depends on the number of reacting molecules and the reaction rate coefficient written above the arrow. In this case the coefficient is multiplied by the number of combinations in which the molecules can assemble. Reaction (4) is used to model the addition of monomers to the system. As $k_{\text{feed}}(t)$ we define the rate at which we add monomers at a certain time t. Although, here k_{feed} is a fixed constant, the addition rate can be varied over time. Following the work of Gillespie,[23] the rate equations for all reactions are the following

$$\mathrm{R}_1(s,r) = \begin{cases} k_\mathrm{p}\cdot(s+r)\cdot[\mathrm{AB}_s]\cdot[\mathrm{AB}_r] & ,s\neq r \\ k_\mathrm{p}\cdot 2\cdot s\cdot\dfrac{[\mathrm{AB}_s]^2}{2} & ,s=r \end{cases} \tag{5}$$

$$\mathrm{R}_2(s,r) = k_\mathrm{p}\cdot s\cdot[\mathrm{B}_s]\cdot[\mathrm{AB}_r] \tag{6}$$

$$\mathrm{R}_3(s) = k_\mathrm{c}\cdot s\cdot[\mathrm{AB}_s] \tag{7}$$

$$\mathrm{R}_4 = k_{\text{feed}} \tag{8}$$

In agreement with previous studies[13,19,24,25] the following system of ordinary differential equations (ODE) can be derived from the reaction rates.

$$\begin{aligned}\frac{\mathrm{d}[\mathrm{AB}_s]}{\mathrm{d}t} = {} & \frac{k_\mathrm{p}}{2}s\sum_{r=1}^{s-1}[\mathrm{AB}_{s-r}][\mathrm{AB}_r] \\ & - k_\mathrm{p}[\mathrm{AB}_s]\left(s\mu_0^{\mathrm{AB}} + \mu_1^{\mathrm{AB}}\right) - k_\mathrm{p}[\mathrm{AB}_s]\mu_1^{\mathrm{B}} \\ & - \left(1-\delta_{s,1}\right)k_\mathrm{c}s[\mathrm{AB}_s] + \delta_{s,1}k_{\text{feed}}\end{aligned} \tag{9}$$

$$\begin{aligned}\frac{\mathrm{d}[\mathrm{B}_s]}{\mathrm{d}t} = {} & \left(1-\delta_{s,1}\right)k_\mathrm{c}s[\mathrm{AB}_s] \\ & + \left(1-\delta_{s,1}\right)k_\mathrm{p}\sum_{r=1}^{s-1}(s-r)[\mathrm{B}_{s-r}][\mathrm{AB}_r] \\ & - k_\mathrm{p}s[\mathrm{B}_s]\mu_0^{\mathrm{AB}}\end{aligned} \tag{10}$$

$[\mathrm{AB}_s]$ and $[\mathrm{B}_s]$ are the concentrations of the respective polymers, and the kth moment for the polymer size distributions is defined as

$$\mu_k^{\mathrm{AB}} = \sum_{s=1}^{\infty} s^k\cdot[\mathrm{AB}_s] \tag{11}$$

and

$$\mu_k^{\mathrm{B}} = \sum_{s=1}^{\infty} s^k\cdot[\mathrm{B}_s] \tag{12}$$

The Kronecker symbol, $\delta_{i,j}$, is defined as

$$\delta_{i,j} = \begin{cases} 1 & ,i=j \\ 0 & ,i\neq j \end{cases} \tag{13}$$

In the beginning, since the reactor contained only solvent, we initialized the system with $\mathrm{AB}_s = \mathrm{B}_s = 0$ for all s. As a result, the system dynamics could be simulated by solving this system as an initial value problem. The temperature and pressure were kept constant throughout each simulation, but the change in volume had to be accounted for in order to update the concentrations correctly. The problem was solved by the simulation software PREDICI.

The described model has two degrees of freedom in the form of the reaction rate coefficients k_p and k_c. The parameter estimation procedure provided by the PREDICI software was used to solve the minimization problem which was to find those parameter values for which the difference between experimental data and simulation result is minimal. This problem was solved via a sophisticated, damped Gauss-Newton method which is very sensitive to the initial values for the estimation.[26] In order to find good starting values, we performed a parameter variation analysis and compared the simulated values for $\overline{M}_\mathrm{n}$ and $\overline{M}_\mathrm{w}$ to the experimental data measured with the GPC.

4. Results and Discussion

4.1. Experimental Results

Studying the results from the MALDI-TOF-MS characterization, one clearly observes a series of peaks corresponding to the molecular weights of the *d*PG polymers of different sizes (Figure 1). In order to identify the discrete polymer size distribution (PSD) we used the OpenMS software.[27] After performing a baseline reduction and filtering out the noise, the build-in peak picking procedure resulted in a discrete molecular mass distribution (MMD). Most of the molar masses could clearly be associated with polymers of different sizes, but some peaks could not be assigned. Most of the unidentified signals were very low due to noise. However, some distinct signals could also be found which may be artifacts of the measurement (e.g., matrix or impurities).

The mass spectra clearly prove the formation of oligomers in the absence of catalysts. Therefore, thermal

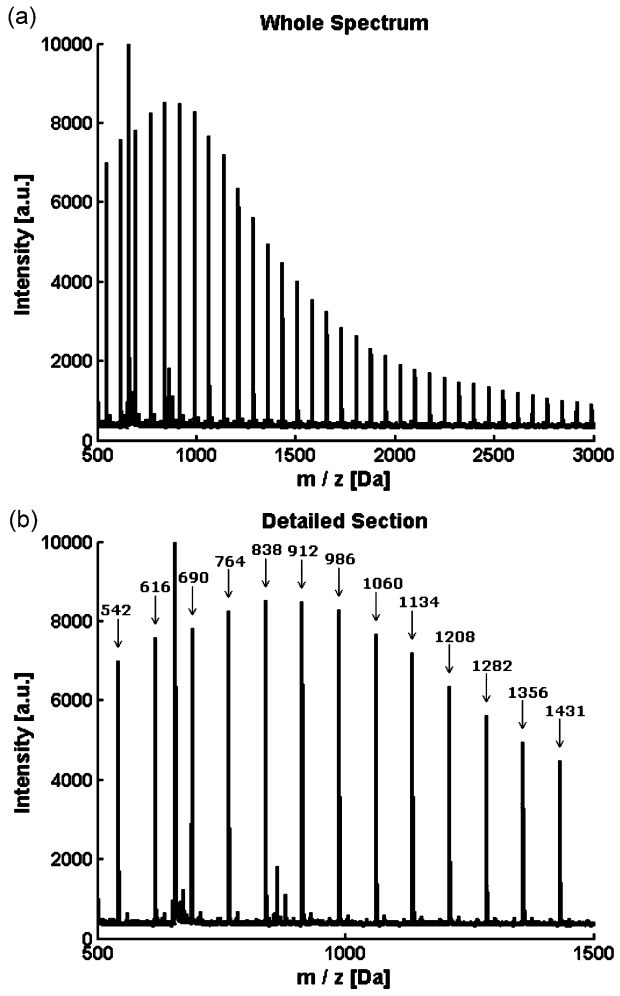

Figure 1. Complete MALDI-TOF mass spectrum (a) for the final sample (reaction time $t = 18$ h) of the experiment at 105 °C. A detailed inspection (b) shows a series of distinct peaks that can be associated with polymers of different sizes.

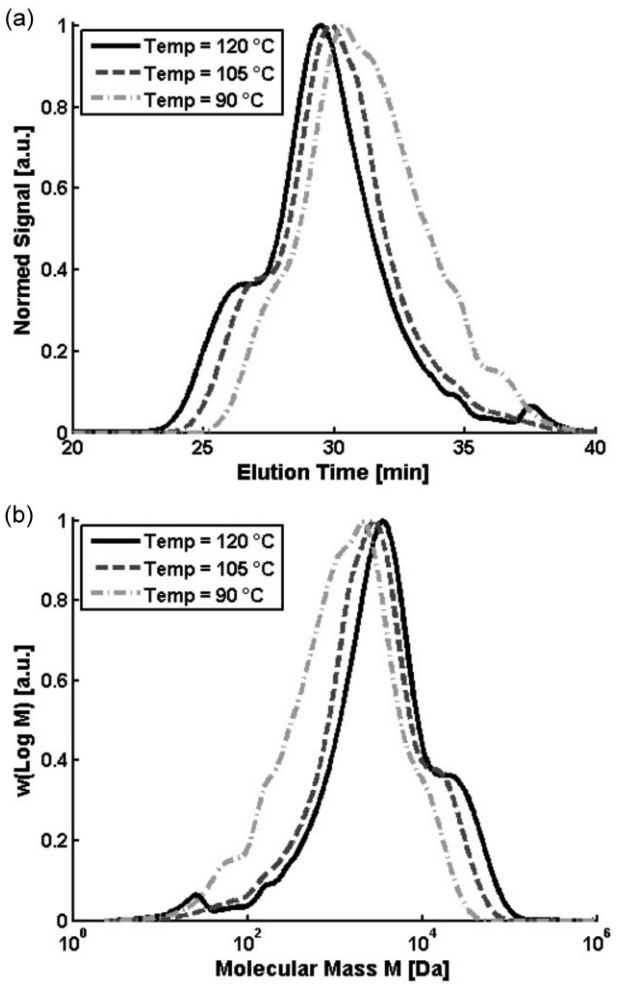

Figure 2. (a) Observed elution time diagram of the final samples (reaction time $t = 18$ h) at different temperatures and (b) molecular mass distributions calculated from the elugrams with help of the calibration curve.

ring-opening reactions have to be considered at elevated temperatures. Unfortunately, this characterization method cannot capture all of the polymers due to the signal interference caused by the dispersity of the polymers.[28] The resulting MALDI-TOF MS data was therefore not used for the computational analysis of the process kinetics.

The NMR measurements can be used to assess the molecular structure of the polymers. After a close inspection of the data, we could see that there were around 2.5 times more secondary hydroxyl groups attached to the polymer's backbone than primary ones. This indicates that primary hydroxyl derivatives are used up more frequently due to a higher reactivity. However, since the ratio between these types of hydroxyl groups did not significantly change throughout the polymerization, we can still estimate the overall ring-opening reaction rate with a single coefficient. Thus, the coefficient k_p depicts the effective reaction rate rather than the elemental ring-opening reaction rate, but is useful for the parameter estimation procedure nonetheless.

The most promising data is produced by the GPC method which is known to be the most reliable source for obtaining average molecular weights and polydispersities. These values were obtained by using pullulan and dextran standards to transform the GPC elugrams (shown in Figure 2a) into MMDs (Figure 2b). We used the calibration curve obtained through the linear standard (pullulan) because it is more accurate for small molecules, but one can also obtain similar results when using the branched standard (dextran) and the differences are within the measurement error. The markers in Figure 3 shows the calibration signals (pullulan and dextran) and the regression curve used to translate elution time into molar mass.

The number-average molecular weight ($\overline{M}_n$), weight-average molecular weight ($\overline{M}_w$) and the PDI for all samples

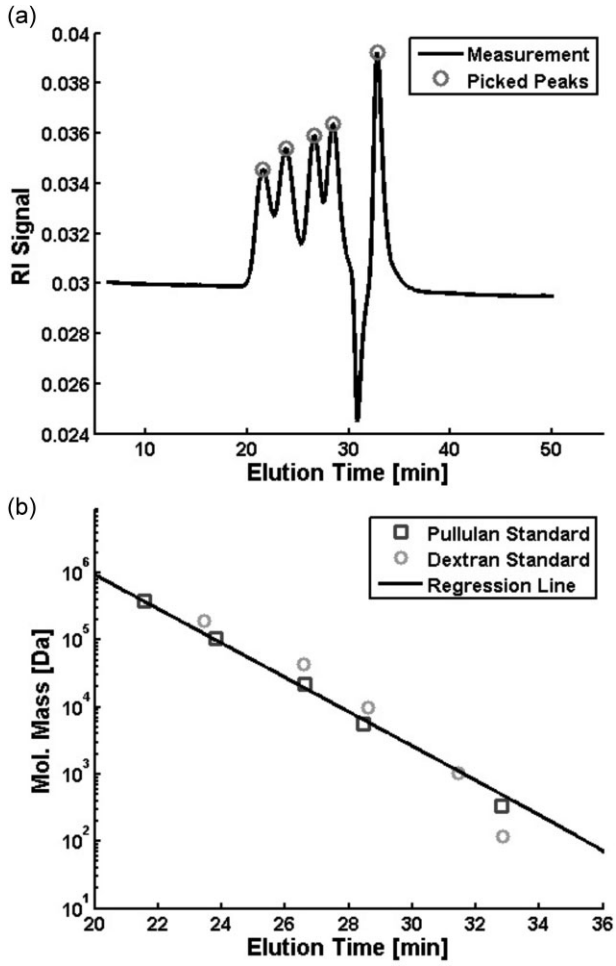

Figure 3. (a) Elution time diagram of the pullulan standards and (b) the calibration curve based on the two types of standards. Squares show the signal for the pullulan standards (linear), circles for the dextran standards (branched), and the line represents the regression curve used for obtaining average molecular masses.

across the three reaction temperatures investigated can be seen in Table 1.

A detailed analysis of the GPC data indicates a strong dependency of the average molecular weight on the reaction temperature. Values for $\overline{M}_n$ from the experiments at 120 °C are almost three times higher than those obtained at 90 °C. The polydispersity, on the other hand, reached a high value in all cases. After 12 h, the PDI was very high for all samples and the values did not differ significantly (between 5.01 and 7.11). However, a higher reaction temperature always introduced a slight increase of the PDI.

We can clearly see the formation and growth of polymers due to thermal ring-opening reactions. The high dispersity is reason enough to suppress these reactions, but a crucial fact is that monomers can combine spontaneously so that the total number of polymers in the system cannot be controlled perfectly. Even though adding highly reactive initiators to the system will prevent most of the monomers from reacting with hydroxyl groups, these side reactions will always contribute to the overall dynamics, especially when the hydroxyl groups vastly outnumber the active sites (i.e., deprotonated hydroxyl groups). Therefore, simulating the reaction kinetics of any polymerization process based on glycidol is not possible without knowing the kinetic parameters for the thermal ring-opening reactions.

4.2. Simulation Results

We started our investigation by testing a broad variety of parameter values ranging over 20 orders of magnitude. Therefore, we performed simulations for many different combinations of parameter values. The results were qualitatively analyzed by comparing the simulated values for $\overline{M}_n$ and $\overline{M}_w$ to the measurements. Unfortunately, the simulation software becomes highly instable for low cyclization rates (k_c) in combination with high propagation rates (k_p). This is due to the fact that in these cases almost all polymers in the system can combine with each other and larger polymers react faster than small ones. A drastic broadening and tailing of the PSD increases the numerical error up to a critical point where the software is not able to compensate anymore and the simulation has to be aborted. We also observed a steep increase in average molecular weight, which should have resulted in the formation of a gel. Since we did not observe this behavior in the experiments, these parameter combinations were negligible. However, for the completeness of the parameter variation analysis, we modified the model slightly in order to get an idea about the system's behavior for non-processable parameter values. For the modified model we fixed the maximal size of non-cyclic polymers. We used a cut-off value of 12 and disregarded all reactions that would have created AB_m polymers of size 13 or bigger. Eliminating only polymer propagations and combinations, we know that the average molecular weights obtained by the thus modified model are always lower or equal to the values obtained with the complete model. The simulation results for $\overline{M}_n$ and $\overline{M}_w$ were higher than the measured ones for the modified model and therefore also for the complete model. In order to find the optimal parameters we measured the difference between simulation results and experimentally observed data of $\overline{M}_n$ and $\overline{M}_w$ by means of the residual, i.e., the weighted root mean sum of squares of the respective deviations. For most parameter combinations one observes quite large residuals, but in a small region ($10^{-5}\,L\cdot mol^{-1}\cdot s^{-1} < k_p < 10^{-4}\,L\cdot mol^{-1}\cdot s^{-1}$ and $10^{-5}\,s^{-1} < k_c < 10^{-4}\,s^{-1}$) very low values were obtained. This region was investigated more closely. Fortunately, the complete model performed reasonably well for this region

Table 1. Summary of GPC measurements for experiments performed at temperatures of 120, 105, and 90 °C. Samples were taken every 2 h and after the reaction had been stopped. Presented are the obtained values for the number- and weight-average molecular weights together with the dimensionless PDI.

Sample time [h]	120 °C			105 °C			90 °C		
	$\overline{M}_n$ [g · mol^{-1}]	$\overline{M}_w$ [g · mol^{-1}]	PDI	$\overline{M}_n$ [g · mol^{-1}]	$\overline{M}_w$ [g · mol^{-1}]	PDI	$\overline{M}_n$ [g · mol^{-1}]	$\overline{M}_w$ [g · mol^{-1}]	PDI
2 h	117.8	233.5	1.98	101.6	227.2	2.24	131.9	548.6	4.16
4 h	336.1	1 550.0	4.61	235.7	841.8	3.57	116.6	173.3	1.49
6 h	486.6	2 889.3	5.94	365.0	1 599.1	4.38	133.8	231.9	1.73
8 h	639.1	3 681.1	5.76	456.9	2 274.8	4.98	238.2	907.3	3.81
10 h	806.4	4 777.4	5.92	558.0	2 935.2	5.26	283.6	1 202.9	4.24
12 h	873.8	5 919.2	6.77	640.8	3 773.7	5.89	342.4	1 716.6	5.01
14 h	979.0	6 303.0	6.44	749.6	4 360.2	5.82	393.0	2 120.5	5.40
16 h	1 127.0	7 926.4	7.03	829.4	5 175.5	6.24	436.6	2 533.6	5.80
18 h	1 268.3	9 014.4	7.11	899.1	5 727.9	6.37	488.3	2 917.1	5.97
final	n/a	n/a	n/a	978.1	5 824.6	5.96	505.3	2 993.5	5.92

in parameter space and both models produced nearly identical results. Therefore, we abandoned the modified model and used the complete model in all subsequent steps.

The aim was to find optimal Arrhenius parameters $A(k_p)$, $E_a(k_p)$, $A(k_c)$, and $E_a(k_c)$ defining the temperature dependency of k_c and k_p via the Arrhenius equation

$$k = A(k)\cdot\exp\left(-\frac{E_a(k)}{RT}\right) \tag{14}$$

where T is the reaction temperature, A is known as prefactor, and E_a is the activation energy. R represents the universal gas constant. There are two different approaches to obtain these parameters: (1) one first finds the optimal values for k_c and k_p independently for each of the three reactor temperatures and then determines the Arrhenius parameters by means of a regression using the Arrhenius equation, or (2) use the parameter estimation tool of PREDICI to identify the Arrhenius parameters directly. We performed both approaches successively since the direct approach (2) is rather nonlinear and tends to cause convergence problems with the parameter estimation procedure if the initial parameter guesses are not good enough.

In order to realize approach (1), we started with the "boxsearch" feature implemented in PREDICI to quickly compare the simulations with promising parameter values to the measurements of all three experiments separately. The parameter variation provided good initial parameter values which we used to perform the residual oriented parameter estimation procedure provided by the PREDICI package with automatic projection. We obtained three parameter pairs (k_p,k_c), one for every experiment at temperatures of 90, 105, and 120 °C. With these parameters we could generate Arrhenius plots as illustrated in Figure 4 and assert the Arrhenius parameters $A(k_p)$, $E_a(k_p)$, $A(k_c)$, and $E_a(k_c)$ by means of regression.

Next we improved the accuracy of the Arrhenius parameters by performing the direct parameter estimation approach (2). We used a feature of PREDICI that allows one to estimate all four Arrhenius parameters directly by fitting the experimental data for all temperatures at the same time. This optimization problem is much more complex than the ones solved before and we had to use the

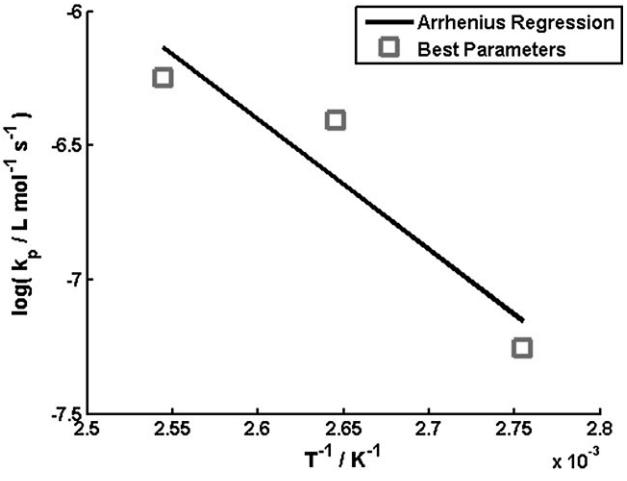

Figure 4. Arrhenius plot for k_p. The markers indicate the optimal values for the three reaction temperatures. The solid line shows the result of the linear regression.

Table 2. Summary of the estimated parameters. The best pair of parameters k_p and k_c obtained in the variation analysis (row I) was used as initial guess for estimating optimal parameters for the three experiments individually (row II). For these parameters an Arrhenius expression with prefactor A and activation energy E_a were obtained by linear regression of the Arrhenius plot (row III). The Arrhenius parameters from the linear regression served as an initial guess for the direct approach using the fitting procedure of PREDICI (row IV).

Analysis	k_p					k_c				
	A [L · mol^{-1} · s^{-1}]	E_a [J · mol^{-1}]	k_p [L · mol^{-1} · s^{-1}]			A [s^{-1}]	E_a [J · mol^{-1}]	k_c [s^{-1}]		
			120 °C	105 °C	90 °C			120 °C	105 °C	90 °C
I	n/a	n/a	3.54×10^{-5}	2.81×10^{-5}	1.12×10^{-5}	n/a	n/a	4.45×10^{-5}	5.60×10^{-5}	2.23×10^{-5}
II	n/a	n/a	3.23×10^{-5}	2.75×10^{-5}	1.17×10^{-5}	n/a	n/a	3.80×10^{-5}	5.19×10^{-5}	2.62×10^{-5}
III	8.26	4.04×10^{4}	3.61×10^{-5}	2.21×10^{-5}	1.30×10^{-5}	4.93×10^{-3}	1.54×10^{4}	4.51×10^{-5}	3.74×10^{-5}	3.06×10^{-5}
IV	8.26	4.04×10^{4}	3.50×10^{-5}	2.14×10^{-5}	1.26×10^{-5}	4.92×10^{-3}	1.55×10^{4}	4.28×10^{-5}	3.55×10^{-5}	2.89×10^{-5}

knowledge gained form approach (1) for choosing good initial values to make sure that the direct method converged. The final results of the two approaches are summarized in Table 2. Rows I and II show the best parameter values from approach (1) after the parameter variation and estimation, respectively. In the last two rows, the Arrhenius parameters after regression from approach (1) and Arrhenius optimization using approach (2) are shown. The values for k_p and k_c in rows III and IV were calculated with the respective Arrhenius parameters and temperatures. The final residual is around 0.12 and indicates a very accurate description of the experimental data.

Figure 5 summarizes both approaches to estimate optimal Arrhenius parameters. The contour plots show the residual landscapes in the parameter space. The region indicated by the light gray contour yields parameter combinations that produce results very close to the measured values (total residual is less than 0.2). The circle markers indicate the optimal parameter values obtained when fitting the experimental data sets individually and the cross markers were calculated with the optimal Arrhenius parameters obtained through the direct parameter estimation procedure.

Finally, in Figure 6 we present the simulated time profiles of $\overline{M}_n$ and $\overline{M}_w$ (obtained by using the optimized Arrhenius parameters) at different temperatures. Comparing the simulation results (solid lines) to the measured values (markers), we can see good agreement of the results. The only significant difference can be observed when inspecting the results at 90 °C. The first three values measured for $\overline{M}_n$ and $\overline{M}_w$ show an unpredictable behavior. This indicates that the GPC characterization technique is not suitable for the detection of very small molecules like monomers, dimers, and trimers.

The aim of this study was to derive a base model that can be used to improve the polymerization of glycidol in the presence of anionic initiators. Therefore, a simplified model was derived that can be extended by incorporating anionic ring-opening reactions and ion transfer reactions. However, the model is not limited to this purpose. It can also be extended in different ways to capture the elemental chemical mechanics more precisely, e.g., a more complex cyclization rate coefficient depending on the distance between the polymer's reacting groups or the distinction between primary and secondary hydroxyl groups. However, such extensions are only useful after extensive analysis of the polymers' structure and since the experimental data was reproduced so accurately by the simplified model, there is not benefit in using a more complex model.

5. Conclusion

The experimental data clearly indicates the formation of oligomers at elevated temperatures even at high dilution. This implies that thermal ring-opening reactions cannot be disregarded when analyzing the polymerization of glycidol at higher temperatures. Not only do they affect the propagation rates, they also lead to the spontaneous combination of monomers which does not allow control of the overall number of polymers in the system. In this study, we derived a simplified mathematical model based on the thermal ring-opening mechanics of glycidol and we used it to performed simulations with the software PREDICI. Arrhenius parameters were estimated for the rate coefficients of thermal ring-opening reactions, including the intermolecular combination reactions (k_p) for monomers and polymers, as well as for the intramolecular cyclization reactions (k_c). The proposed model is capable of simulating reactions at different temperatures and the results are in excellent agreement with the experimental data.

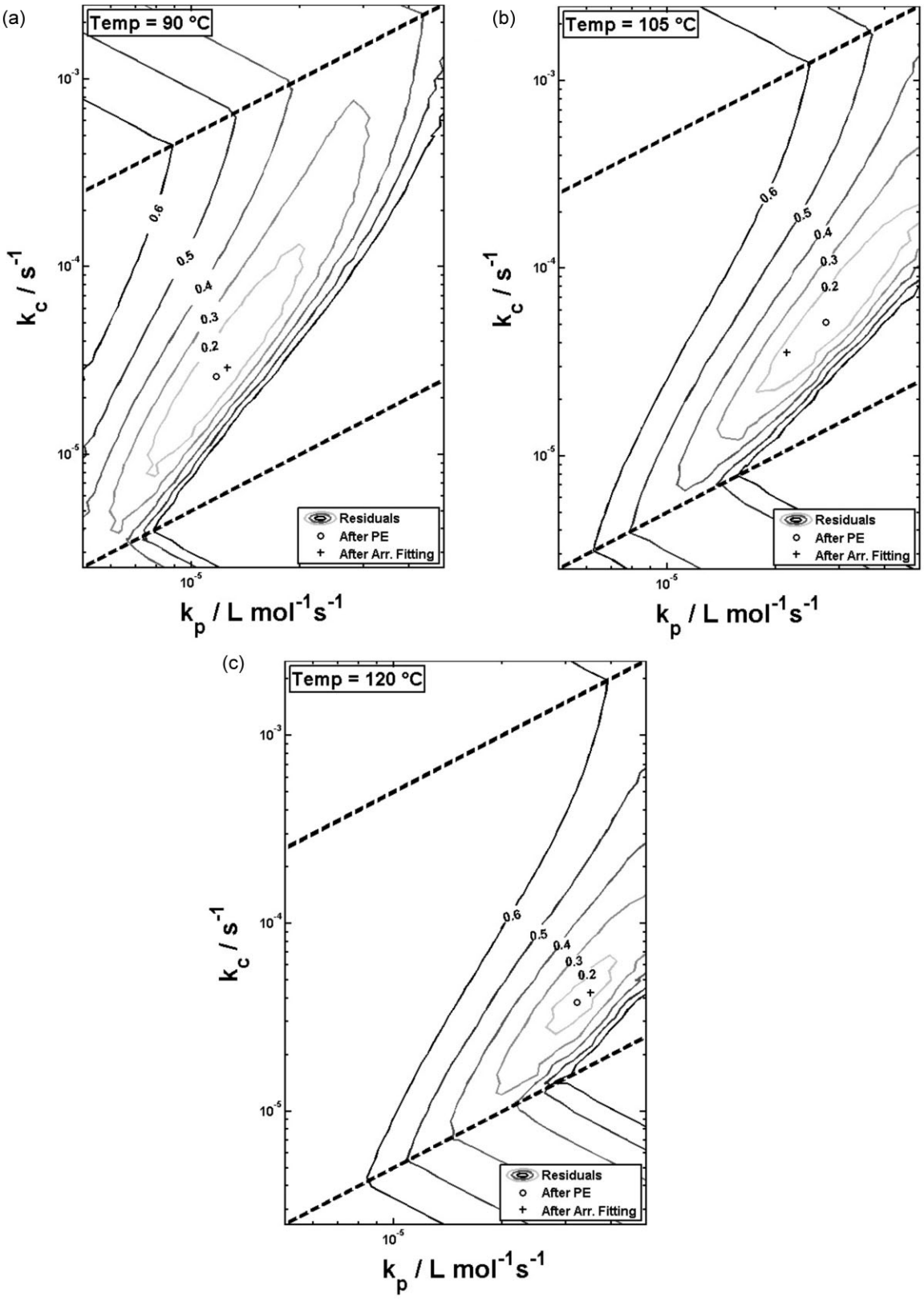

Figure 5. Contour plot of the residuals for the three experiments at (a) 90, (b) 105, and (c) 120 °C. The markers indicate the optimal parameter values after the individual parameter estimation (circles) and after the final fitting of the Arrhenius parameters (crosses).

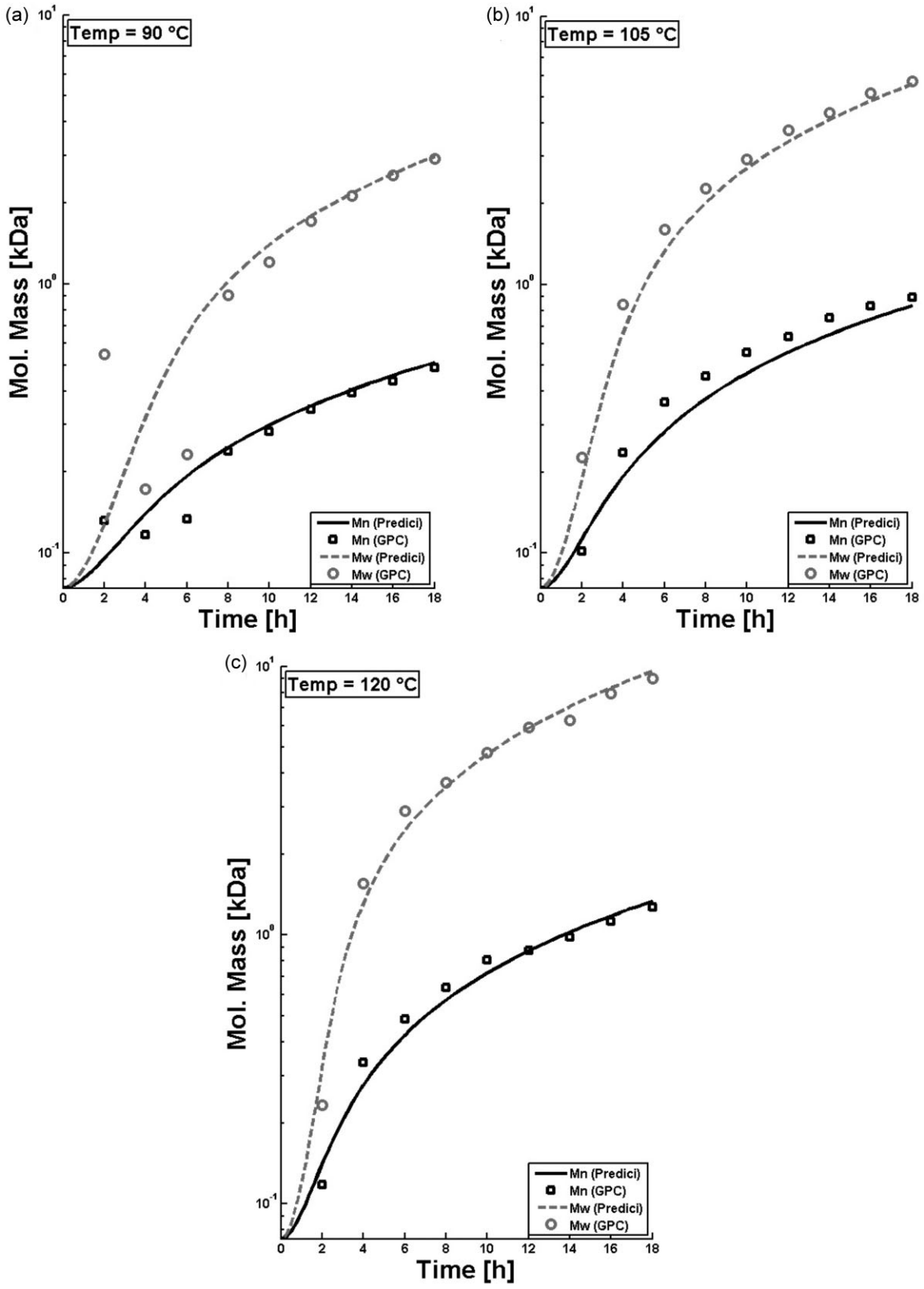

Figure 6. Time profiles of the number- and weight-average molecular weights ($\overline{M}_n$, $\overline{M}_w$) on a logarithmic scale. Markers represent the measured data and the solid lines were simulated with the optimal Arrhenius parameters at different temperatures of (a) 90, (b) 105, and (c) 120 °C.

Estimating the kinetic parameters for this comparatively simple polymerization process allows simulation of more complex models that incorporate partially deprotonated initiators by extending the system of reaction equations with anionic ring-opening and ion transfer reactions. This study was a vital step toward simulating the synthesis of polyglycerol because the problem is too complex to be solved directly without prior knowledge about the thermally induced ring-opening reactions. We are now able to employ mathematically controlled process optimization methods that can be used to synthesize products of better quality with less effort.

Acknowledgements: We thank Dr. Michael Wulkow for providing the PREDICI software and for many helpful discussions. Financial support by the Dahlem Research School is gratefully acknowledged.

Received: January 5, 2012; Revised: March 7, 2012; Published online: June 13, 2012; DOI: 10.1002/mats.201200003

Keywords: computer modeling; dendritic polyglycerols; parameter estimation; predici; ring-opening polymerization

[1] E. J. Vandenberg, *J. Polym. Sci., Part A: Polym. Chem.* **1985**, *23*, 915.
[2] H. Frey, R. Haag, *Rev. Mol. Biotechnol.* **2002**, *90*, 257.
[3] D. Wilms, S.-E. Stiriba, H. Frey, *Acc. Chem. Res.* **2010**, *43*, 129.
[4] J. Dernedde, I. Papp, S. Enders, S. Wedephol, F. Paulus, R. Haag, *J. Carbohydr. Chem.* **2011**, *30*, 347.
[5] K. Licha, C. Hessenius, A. Becker, P. Henklein, M. Bauer, S. Wisniewski, B. Wiedenmann, W. Semmler, *Bioconjug. Chem.* **2001**, *12*, 44.
[6] Y. H. Kim, O. W. Webster, *J. Am. Chem. Soc.* **1990**, *112*, 4592.
[7] J. Frechet, *React. Funct. Polym.* **1995**, *26*, 127.
[8] S. R. Sandler, F. R. Berg, *J. Polym. Sci., Part A: Polym. Chem.* **1966**, *4*, 1253.
[9] R. Tokar, P. Kubisa, S. Penczek, A. Dworak, *Macromolecules* **1994**, *27*, 320.
[10] A. Dworak, W. Walach, B. Trzebicka, *Macromol. Chem. Phys.* **1995**, *196*, 1963.
[11] A. Sunder, R. Hanselmann, H. Frey, R. Mülhaupt, *Macromolecules* **1999**, *32*, 4240.
[12] P. J. Flory, *J. Am. Chem. Soc.* **1952**, *74*, 2718.
[13] W. Radke, G. Litvinenko, A. H. E. Müller, *Macromolecules* **1998**, *31*, 239.
[14] R. Hanselmann, D. Hölter, H. Frey, *Macromolecules* **1998**, *3*, 3790.
[15] A. Burgath, A. Sunder, H. Frey, *Macromol. Chem. Phys.* **2000**, *201*, 782.
[16] W. H. Ray, *J. Macromol. Sci., Polym. Rev.* **1972**, *8*, 1.
[17] M. Busch, M. Müller, M. Wulkow, *Chem. Eng. Technol.* **2003**, *26*, 1031.
[18] M. Wulkow, *Macromol. React. Eng.* **2008**, *2*, 461.
[19] M. Wulkow, *Macromol. Theory Simul.* **1996**, *5*, 393.
[20] H. Türk, S. Mecking, R. Haag, (Hyperpolymers GmbH), DE 10211664 A1, 2003.
[21] H. Jacobson, W. H. Stockmayer, *J. Chem. Phys.* **1950**, *18*, 1600.
[22] R. Hendrickson, A. Gupta, C. W. Macosko, *Comp. Polym. Sci.* **1995**, *5*, 1.
[23] D. T. Gillespie, *J. Phys. Chem.* **1977**, *81*, 2340.
[24] R. Szymanski, *Macromol. Theory Simul.* **2011**, *20*, 8.
[25] K. Dušek, J. Šmovársky, M. Smrčková, W. J. Simonsickm, Jr., L. Wilcez, *Polym. Bull.* **1999**, *42*, 489.
[26] P. Deuflhard, *Newton Methods for Nonlinear Problems – Affine Invariance and Adaptive Alforithms*, 1st edition, *Vol. 35*, Springer Series in Computation Mathematics, Springer, Heidelberg **2004**.
[27] M. Sturm, A. Bertsch, C. Gröpl, A. Hildebrandt, R. Hussong, E. Lange, N. Pfeifer, O. Schulz-Trieglaff, A. Zerck, K. Reinert, O. Kohlbacher, *BMC Bioinf.* **2008**, *9*, 163.
[28] M. W. F. Nielen, S. Malucha, *Rapid Commun. Mass Spectrom.* **1997**, *11*, 1194.